*particles*

MDPI

*Article*

# Thermal Spectrum and Neutrino Cooling Rate of the Vela Pulsar

**Dmitry D. Ofengeim and Dmitry A. Zyuzin**

Ioffe Institute, 26 Politekhnicheskaya str., St. Petersburg 194021, Russia; da.zyuzin@gmail.com
* Correspondence: ddofengeim@gmail.com; Tel.: +7-812-292-7180

Received: 22 June 2018; Accepted: 24 July 2018; Published: 30 July 2018

**Abstract:** We reanalyse the X-ray spectrum of the PSR B0833–45 (the Vela pulsar) using the data of the *Chandra* space observatory. In contrast to previous works, we consider a wide range of possible masses and radii of the pulsar. The derived surface temperature of the star $T_s^\infty = 0.66^{+0.04}_{-0.01}$ MK ($1\sigma$ level over the entire mass and radius range of our study) is consistent with earlier results. However, the preferable values of Vela's mass and radius given by the spectral analysis are different from those used previously; they are consistent with modern equation of state models of neutron star matter. In addition, we evaluate the Vela's surface temperature as a function of assumed values of its mass and radius. This allows us to analyse the neutrino cooling rates consistent with the evaluated surface temperatures and explore the additional restrictions that could be set on the Vela's mass and radius using different versions of the neutron star cooling theory.

**Keywords:** the Vela pulsar; X-ray spectrum; neutrino cooling rate

## 1. Introduction

In this presentation, we reanalyze the observations of the X-ray surface emission of the Vela pulsar (PSR B0833-45) and evaluate its effective surface temperature $T_s^\infty$ (redshifted for a distant observer), mass $M$, radius $R$ and the internal neutrino cooling rate using the cooling theory of neutron stars (NSs) [1].

The Vela is a famous middle-aged pulsar whose emission has been observed at different wavelengths. Its X-ray emission has been observed with a number of space observatories (most importantly, with *Chandra* and *XMM-Newton*). We take its characteristic age as $t \sim 11$ kyr, although it is ambiguous due to frequent glitches (e.g., Lyne [2] obtained $t \sim 25$ kyr); its real age is hard to derive due to irregular shape of the Vela supernova remnant [3]. The magnetic field at the magnetic poles is $B_{\rm surf} \approx 3.38 \times 10^{12}$ G [4] (http://www.atnf.csiro.au/people/pulsar/psrcat/), and the parallax distance to the pulsar is $d = 287^{+19}_{-17}$ pc [5]. The surface temperature has been estimated as $T_s^\infty \approx 0.7$ MK (using the *nsa* atmosphere model [6] with a power-law non-thermal component and assuming $M = 1.4\,M_\odot$ and $R = 10$ km [7–9]).

By inferring $T_s^\infty$ from observations and using the NS cooling theory, one can constrain most important parameters of the star including fundamental properties of superdense matter in its interior. We will use the cooling theory of NSs with nucleon cores and not too strong magnetic fields (to avoid dramatic effects of the $B$-fields on the NS structure and evolution, such as considered in [10–12]). Figure 1 shows some theoretical cooling curves ($T_s^\infty$ versus age $t$) compared with the observations of such (not highly magnetized) NSs. The curves are calculated using the approximate analytic expressions [13] for a $1.4\,M_\odot$ star. The stars of age $t \gtrsim 10$–$100$ yr are thought to be thermally relaxed inside with a noticeable temperature gradient remaining only in a thin surface layer called the heat blanketing envelope (e.g., [14–16]). The stars with $t \lesssim 10^5$ yr (including the Vela pulsar) are believed to be cooling predominantly via the neutrino emission from their superdense cores. Older stars cool mostly through their thermal surface emission. The central black solid line shows the standard

cooling [17] (of non-superfluid NSs with the modified Urca neutrino emission in the core and iron heat blanketing envelope). This curve is almost unaffected by the equation of state (EOS) of NS matter and NS mass (e.g., [18]). The dot-and-dashed curve is the same, but the neutrino emission is enhanced by a factor of 100 (e.g., by neutrinos produced via triplet-state Cooper pairing of neutrons in a superfluid core, see Section 3). The dashed curve is for the NSs with the neutrino emission reduced by a factor of 100 (for instance, by strong proton superfluidity in the core) and the envelope made of carbon (light elements in the heat blanket reduce its thermal insulation). According to Figure 1, the Vela's neutrino cooling is one of the fastest among the observed NSs, making the Vela especially interesting.

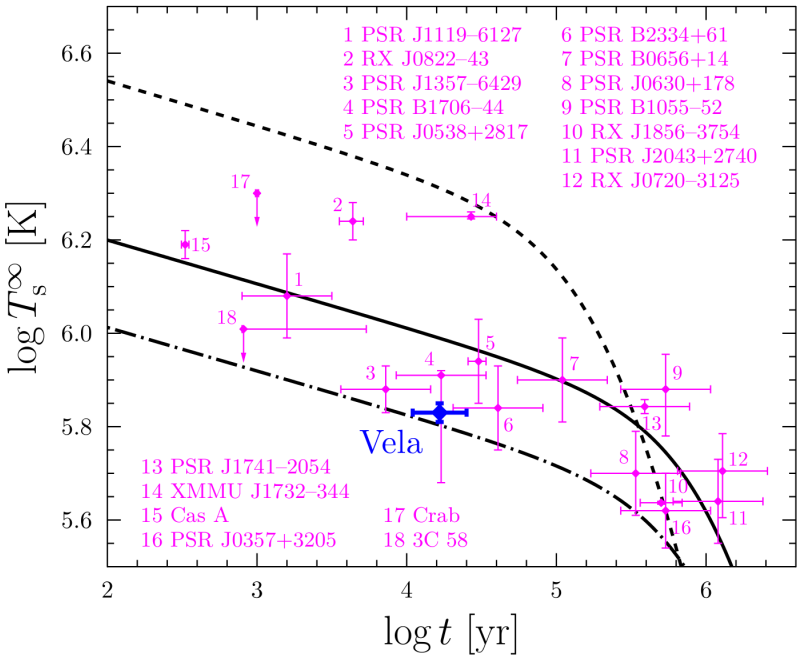


**Figure 1.** Theoretical cooling curves $T_s^\infty(t)$ compared with observations of 19 cooling NSs. Temperatures and ages are taken from Table 1 of Ref. [19]. Black curves schematically show three cooling scenarios: the solid curve is for the standard cooling of the star with the iron heat blanketing envelope; the dashed curve is for the slow cooling (neutrino emission is 100 times weaker than the standard one) with the carbon envelope; the dash-dotted curve is for the enhanced cooling (neutrino emission is 100 times higher than in the standard case) and the iron heat blanket.

This special status of the Vela pulsar has been noticed previously (e.g., [20]). The Vela's spectrum has been analyzed assuming $M = 1.4\,M_\odot$ and $R = 10$ km (e.g., [7]). The internal neutrino cooling rate has also been studied, but again under the same assumptions. Here, we present our preliminary results obtained without fixing $M$ and $R$. A more extensive analysis will be published elsewhere.

## 2. Spectral Analysis of the Vela Pulsar

There are a lot of X-ray observations of the Vela pulsar, but here we use only those performed by the *Chandra* space observatory in the two modes: HRC-S/LETG (ObsID 127 and 1852, taken on 28.01.00 and 12.01.01, respectively) and ACIS-S/HETG/CC (ObsID 131, taken on 11-12.10.99) (blue and red dots in Figure 2, respectively). The ObsID 127 and 131 observations were used in [7]; the latter one has never been used before. These unique data sets were obtained using the Low-Energy and High-Energy Transmission Gratings (LETG and HETG correspondingly). Other *Chandra* observations of the Vela pulsar are either oriented for timing and spatial analyses or strongly pile-uped, which make them inappropriate for our purposes. The Vela's spectrum was also observed with the *XMM-Newton* observatory [8,9]. We intend to analyze these data in the future.

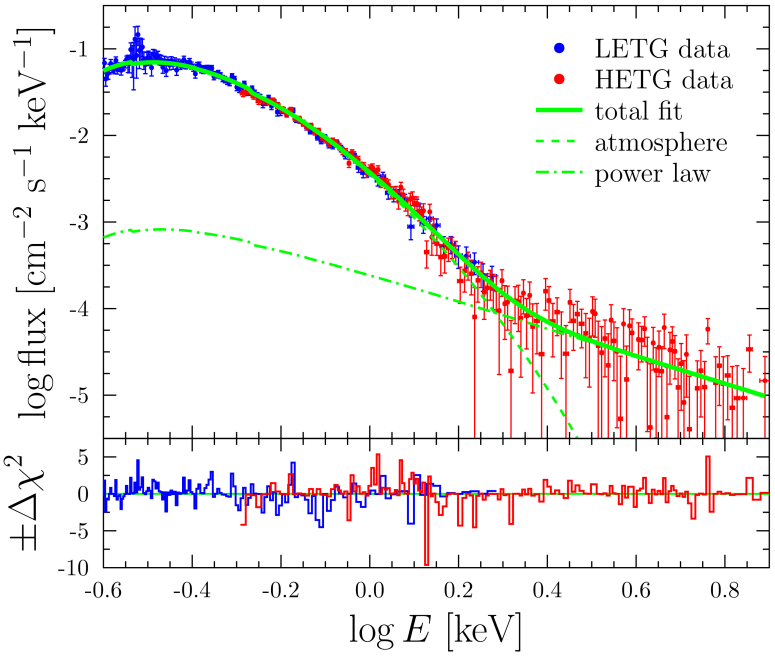


**Figure 2.** The X-ray unfolded spectrum of the Vela pulsar (red, blue) and the fit obtained using the '*nsmax* + power law' model at $M = 1.4\,M_\odot$ and $R = 13$ km (green). Blue dots show the data observed in the HRC-S/LETG mode; red dots are for the ACIS-S/HETG/CC mode. The solid blue line shows the total fit model, while the dashed line is for the *nsmax* model, and the dash-dotted line is for the power-law tail; absorption is included. The bottom panel presents the fit errors ($\Delta\chi^2$ with the sign of the 'data minus model' difference.)

The spectrum is extracted and analyzed with the `ciao` [21] and `sherpa` [22] packages. The source and background extractions are performed as described in Section 2 of [7]. To avoid the contamination by the pulsar wind nebula, for the ACIS-S/HETG/CC observations, we use only the zero-order image for the spectrum extraction. The spectra are grouped to ensure at least 25 counts per energy bin. We fit it, by a combined model, which includes the thermal component described by the *nsmax* [23] model 1230 (magnetic hydrogen atmosphere with the field strength at the pole $2 \times 10^{12}$ G), and the non-thermal component described as a power-law tail. The absorption has been accounted for by the *tbabs* model.

A note should be made on the magnetic field strength used for the spectral analysis. The real Vela's surface field may differ from the standard spindown estimate $\sim 3.4 \times 10^{12}$ G within a factor of few, e.g., [24]. While analyzing the Vela pulsar, it would better to test several values of the field. Here take the surface field $2 \times 10^{12}$ G; in the forthcoming paper, we will consider other models.

The employed spectral model has six physical parameters: the local (non-redshifted) surface temperature $T_\mathrm{s} = T_\mathrm{s}^\infty(1+z)$ with $1+z = (1-2GM/(Rc^2))^{-1/2}$ being the redshift factor, the normalization $N = R^2/d^2$, the power law index $\Gamma$ and its normalization $\mathcal{N}_\Gamma$, and the equivalent hydrogen column density $n_H$ along the line of sight. We fit the observed spectrum for a set of fixed $z$ and $N$ (the $z$ step is 0.0425 and the $N$ step is 100 km$^2$/kpc$^2$), which correspond to $1 \leqslant M \leqslant 3\,M_\odot$ and $9 \leqslant R \leqslant 16$ km at fixed $d = 290$ pc. The parameters $T_\mathrm{s}$, $\Gamma$, $\mathcal{N}_\Gamma$ and $n_H$ are set free. The $\chi^2$ criterion is used as a fit goodness.

The green line in Figure 2 shows an example of our fit at $M = 1.4\,M_\odot$ and $R = 13$ km. It results in $T_\mathrm{s}^\infty = 0.700 \pm 0.005$ MK, $\Gamma = 1.7 \pm 0.3$, and $\mathcal{N}_\Gamma$ and $n_H$ are close to the values obtained in [7] at $R = 10$ km. All other values of $M$ and $R$ lead to almost the same $\Gamma$, $\mathcal{N}_\Gamma$, and $n_H$, but $T_\mathrm{s}^\infty$ varies stronger. In this way, we derive the $T_\mathrm{s}^\infty(M,R)$ map from the observed spectrum; it is demonstrated in Figure 3a. Everywhere on this map, the $T_\mathrm{s}^\infty$ fit error is about $\pm 0.005$ MK.

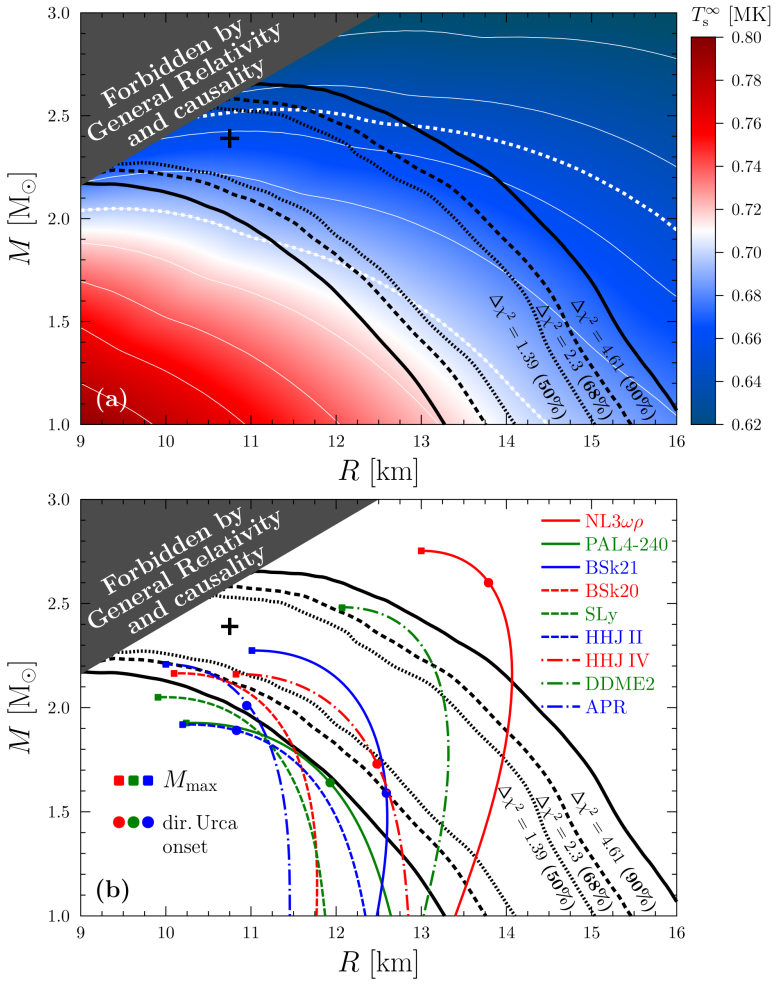


**Figure 3.** (**a**) black contours show the confidence levels for the Vela's $M$ and $R$, derived from the spectral fitting by the '*nsmax* + power law' model, the 'plus' sign shows the best-fit point (see the text for details). Color maps the surface temperature $T_s^\infty$ as a function of $M$ and $R$ inferred from the same analysis. Thin white lines refer to constant $T_s^\infty = 0.62, 0.64, \ldots, 0.78$ MK. Thick white dotted lines show $1\sigma$ bounds on the surface temperature; (**b**) the same confidence levels as on the top figure, but compared to $M - R$ relations for several EOS models (see the text for details). For each EOS, squares mark the maximum-mass stable NS configurations and circles show the NS configurations with the direct Urca process opened just in the stellar center.

Figure 3a shows the best-fit values of $T_s^\infty$ for fixed $M$ and $R$; the minimum $\chi^2$ depends on $M$ and $R$. The confidence levels for the Vela's $M$ and $R$ are plotted in Figure 3a,b by black lines. The best fit (the 'plus' signs in Figure 3) $M = 2.4^{+0.1}_{-1.4}\,M_\odot$ and $R = 10.8^{+3.7}_{-1.3}$ km at $1\sigma$ level (the upper limit for mass and the lower one for radius are obtained from the causality restriction; see the grey-shaded areas in Figure 3) with reduced $\chi^2 = 0.97$ for 294 degrees of freedom. The confidence region for the Vela's temperature over the $(M, R)$ plane (the area within the thick white dotted contours in Figure 3) is $T_s^\infty = 0.66^{+0.04}_{-0.01}$ MK at the $1\sigma$ level. Note that it is close to the results of previous spectral analyses [7–9] including or excluding the *XMM-Newton* data. However, at $M = 1.4\,M_\odot$ and $R = 10$ km, we obtain $T_s^\infty \sim 0.75$ MK, which significantly differs from the temperature obtained in the cited papers for the same $M$ and $R$. This is because the authors of [7–9] treated the distance $d$ as a free parameter; their best-fit $d$ significantly differ from the well-measured parallax distance [5] that we use. In other words, the widely used $T_s^\infty \approx 0.7$ MK does not favors NS models with $M \approx 1.4\,M_\odot$ and $R \approx 10$ km.

Figure 3b compares the Vela's $M-R$ confidence levels and a set of $M-R$ curves for several realistic EOS models. The NL3$\omega\rho$ and DDME2 models belong to the class of relativistic mean field EOSs (described in [25] and in references therein). The APR model is constructed using the variational method [26]. The class of EOSs based on Skyrme-type energy-density functionals is presented by the BSk21, BSk20 [27] and SLy [28] models. The PAL4-240 (also known as PAPAL [29]), HHJ II (also known as APR II [30]) and HHJ IV [31] EOSs constitute the class of semi-analytical models. Some of these EOSs (PAL4-240, SLy, HHJ II, and APR) are not consistent with the restrictions on the Vela's mass and radius given by the 90% confidence level. Other EOSs present many possibilities to be consistent with the Vela's data. This pulsar can be a low-mass NS but with large radius $\sim$13 km. Alternatively, it can be a massive (>1.5 $M_{\odot}$) NS with the radius $\sim$11–12 km that is typical for other NSs with $M$ and $R$ constrained by atmospheric fits [32,33]. It can be even a massive NS with large $R$ that is typical for relativistic mean field EOSs (e.g., [25]).

## 3. Vela's Neutrino Cooling Rate

Let us interpret the Vela's observations using the NS cooling theory. We will employ the method similar to that discussed in [17,20,34] and in references therein. It is well described in the literature; we just outline the main points. Let us assume some values of $M$, $R$ and $T_{\rm s}^{\infty}$ of the star, the chemical composition of the heat blanketing (thermally insulating) envelope, and specify the surface magnetic field $B_{\rm surf} = 3.38 \times 10^{12}$ G. Using the theory of such envelopes, we can determine the internal temperature of the star. Since the Vela pulsar is at the neutrino cooling stage, its cooling is mostly regulated by the neutrino emission from its core. More accurately, it is regulated by the neutrino cooling function $\ell$ which is the ratio of the neutrino luminosity to the heat capacity of the core (the contribution of the stellar crust being unimportant). This cooling function strongly depends on the internal stellar temperature. On the one hand, $\ell$ can be derived if internal temperature and age are determined from observations. On the other hand, it is affected by the NS EOS, $M$ and $R$, as well as by superfluidity of protons and neutrons in the core. Testing different models of $\ell$, one can limit those which are reasonably consistent with observations. All necessary formulae and caveats could be found in [17], Section 4.

The basic model is the standard model of a non-superfluid star cooling via the neutrino emission in the modified Urca process (the modified Urca neutrino emissivity is taken from the classical paper [35]; similar emissivity in the medium-modified approach (e.g., [36]) can be higher; see below). In this standard case, the cooling function $\ell = \ell_{\rm stand}$ can be well approximated by analytic expressions valid in a wide range of $M$ and $R$ for many different EOSs in nucleon cores (e.g., [20]). The cooling curves of such stars, $T_{\rm s}^{\infty}(t)$, are almost independent of $M$ and EOS. This cooling scenario is definitely inconsistent with the observations of the Vela pulsar (Figure 1), which cools faster. Following the method we employ, the real cooling function at the Vela's current cooling stage is approximated as

$$\ell = f_{\ell}\ell_{\rm stand}, \tag{1}$$

where $f_{\ell}$ is a constant at the current stage. The method allows one to find $f_{\ell}$ in such a way that the theoretical $T_{\rm s}^{\infty}(t)$ becomes equal to the value inferred from observations. Thus determined, $f_{\ell}$ contains important information on the NS cooling rate. According to the theory, $f_{\ell}$ can be much larger or much lower than the standard value $f_{\ell{\rm stand}} = 1$ (which would mean a faster or slower neutrino cooling, respectively). The Vela's observations imply $f_{\ell} > 1$, but the specific value depends noticeably on $M$, $R$, and the chemical composition of the heat blanket.

For instance, we can employ the minimal cooling theory [1,30]. It takes into account possible superfluidity of neutrons and protons (via singlet-state and triplet-state pairings, respectively) in NS cores but neglects the very powerful direct Urca process of neutrino cooling (it should be either forbidden by a given EOS or suppressed by superfluidity). A mild neutron superfluidity initiates a specific neutrino cooling due to Cooper pairing of neutrons; it can enhance the cooling factor up to $f_{\ell{\rm max}} \lesssim$ 30–100 (depending mainly on neutron superfluidity models that are highly uncertain).

In addition, the neutrino cooling rate can be enhanced by the in-medium effects in superdense matter (e.g., [36,37]), increasing $f_{\ell\max}$ up to a factor of 300–1000 (see, e.g., figure 4 in [36]).

Another opportunity to rise $f_\ell$ is to allow the direct Urca process to actually operate in the NS core. This can increase $f_{\ell\max}$ up to 5–7 orders of magnitude [18].

Let us try to constrain $f_\ell$ for the Vela pulsar by varying $M$, $R$, and the composition of the heat blanketing envelope. We will use the model of the magnetic heat blankets [14] with $B_{\rm surf} = 3.38 \times 10^{12}$ G at the NS pole, which contain the accreted matter (of light elements) just beneath the NS atmosphere and the iron matter near the heat blanket bottom. The chemical composition is specified by the mass $\Delta M_{\rm acc}$ of the accreted matter. The maximum value $\Delta M_{\rm acc}^{\rm max} \sim 10^{-7}\,M_\odot$ corresponds to the fully accreted heat blanket. At formally higher $\Delta M_{\rm acc}$, the accreted matter at the bottom of the heat blanket would quickly transform into heavier elements via pycnonuclear reactions and beta captures. The value $\Delta M_{\rm acc} \sim 10^{-17}\,M_\odot$ refers to the fully iron (non-accreted) heat blanket.

Assuming the non-accreted heat blanket, we obtain the $f_\ell(M,R)$ relation shown in Figure 4; $f_\ell$ varies strongly inside the confidence contours of the Vela's $M$ and $R$ (Figure 3). Taking the optimistic estimates provided by the minimal cooling paradigm, we should exclude a large piece of the $M-R$ confidence area, which does not satisfy the condition $f_\ell(M,R) \leqslant f_{\ell\max} \lesssim 30$–$40$ (in the log-scale $\lesssim$1.5–1.6). This would lead to the stringent constraints on $M \gtrsim 1.9\,M_\odot$ and $R \lesssim 12.5$ km for the Vela pulsar. Adopting the less stringent approach to the maximal cooling rate within the minimal cooling paradigm, $f_{\ell\max} \sim 60$ ($\log f_{\ell\max} \sim 1.8$), essentially increases the allowable $M-R$ area adding the possibility that the Vela pulsar has a low mass. In principle, we can consider even $f_{\ell\max} \sim 100$, or (combining medium-modified approach with the minimal cooling paradigm) larger ~300–1000, or (by opening the direct Urca process) much higher $f_{\ell\max}$. Then, we obtain that $f_\ell$ (cooling restrictions) cannot constrain $M$ and $R$ at all.

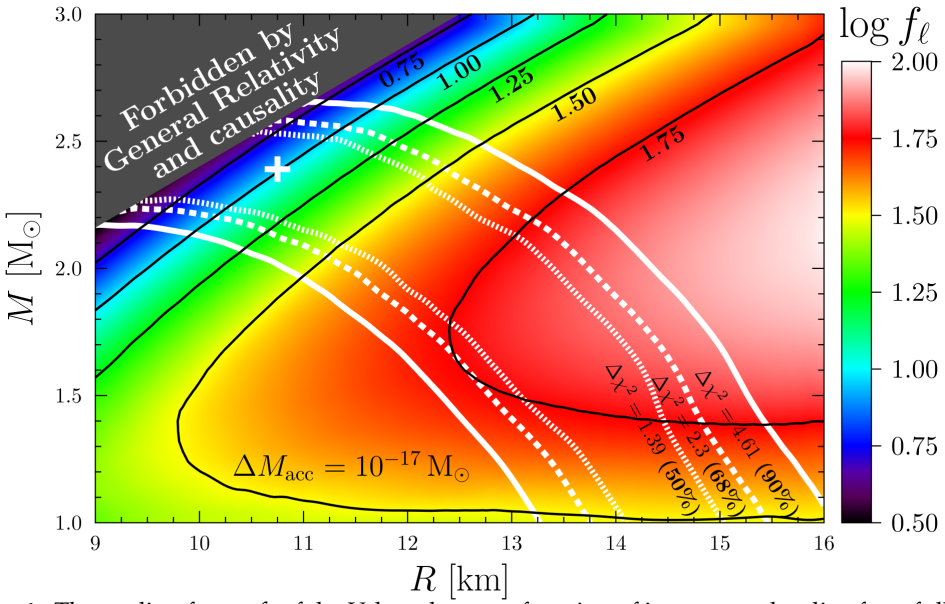


**Figure 4.** The cooling factor $f_\ell$ of the Vela pulsar as a function of its mass and radius for a fully iron heat blanket, $\Delta M_{\rm acc} = 10^{-17}\,M_\odot$. Black lines are the contours of constant $f_\ell$ with $\log f_\ell$ shown near the curves. White lines are the same as in Figure 3a,b.

The presence of the accreted matter in the NS envelope only enlarges $f_\ell$ and changes the cooling restrictions. This is illustrated by Figure 5, where we plot the $f_\ell(M,R)$ map for a moderately accreted crust, $\Delta M_{\rm acc} = 10^{-12}\,M_\odot$. The standard minimal cooling paradigm seems to be helpless for explaining this case. The medium-modified version ($\log f_{\ell\max}$ = 2.5–3) can work out but high- or low-massive stars are preferable. Further increase of $\Delta M_{\rm acc}$ makes the data inconsistent even with the medium-modified approach to the NS cooling.

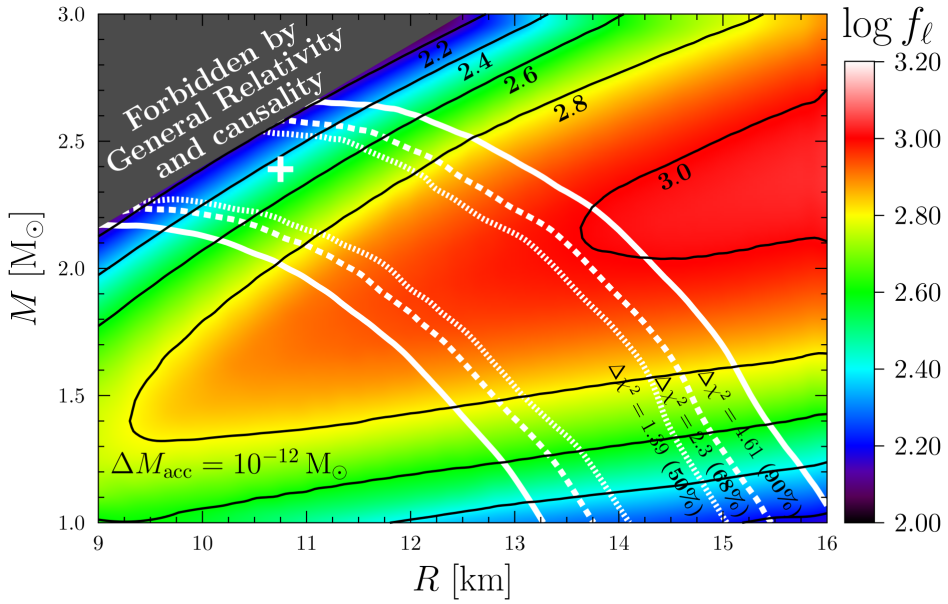


**Figure 5.** The same as in Figure 4 excepted for a moderately accreted heat blanket, $\Delta M_{\rm acc} = 10^{-12}\,M_\odot$.

Therefore, our analysis confirms that the Vela's cooling rate is really higher than the standard one. In the frame of the minimal cooling paradigm, the Vela's heat blanket cannot contain a large fraction of accreted matter. These conclusions are consistent with the earlier results [20] obtained from a more simplified analysis.

## 4. Conclusions

We have analyzed the X-ray spectrum of the Vela pulsar using the data of the *Chandra* observatory. We have derived the confidence regions for mass and radius of the pulsar (see Figures 3) and its surface temperature $T_{\rm s}^{\infty} = 0.66^{+0.04}_{-0.01}$ MK. This temperature is consistent with the previous results [7–9]. Forbidding direct Urca process in the Vela's core, we obtain the cooling factor $f_\ell$, Equation (1), as a function of possible Vela's $M$ and $R$ under different assumptions on the heat blanket composition (Figures 4 and 5). Then, we compare the derived $f_\ell(M, R)$ maps with possible theoretical restrictions on the cooling factor predicted by different scenarios of NS cooling. The main conclusion is that the Vela's cooling can be compatible with the minimal cooling paradigm. If so, the star has either rather large or rather low mass and its heat blanketing envelope is composed of non-accreted or partially accreted matter. Otherwise, the star has the neutrino cooling rate that is higher than the rate provided by the minimal cooling paradigm and the heat blanket can be non-accreted or moderately accreted.

In any case, our results are preliminary and can be elaborated further. First, it would be good to include the *XMM-Newton* data. Second, we have used the hydrogen atmosphere model, but the Vela's atmosphere can contain heavier elements. Third, the employed *nsmax* atmosphere model assumes that the magnetic field in the atmosphere is pure dipole, whereas the real field may have higher multipoles. In addition, we have taken only one value of the atmospheric magnetic field, whereas pulsar field estimates are accurate within a factor of few, and a rigorous spectral analysis would require testing several field values. Fourth, we perform the phase-averaged spectral analysis, while the Vela pulsar emission has a pulsed fraction about 10%, e.g., [9]. The atmosphere model we use neglects polar caps (although they may be important; e.g., [38]). This disadvantage may slightly overestimate the surface temperature, and, consequently, slightly underestimate the neutrino cooling rate. Fifth, we artificially neglect the enhanced cooling by the direct Urca process and by possible appearance of hyperons and other exotic phases of superdense matter in the NS core. We have also not studied the effects of possible deviations of chemical composition from that adopted in the employed model [14] of the heat blanketing envelope. All these effects are certainly beyond the scope of the present paper.

**Author Contributions:** D.A.Z. analysed the *Chandra* data; D.D.O. performed the cooling analysis and wrote the paper.

**Funding:** Research was supported by the Fundamental Research Program of Presidium of the RAS P-3.

**Acknowledgments:** We are grateful to Dmitry Yakovlev for our discussion with him.

**Conflicts of Interest:** The authors declare no conflict of interest.

## Abbreviations

The following abbreviations are used in this manuscript:

| | |
|---|---|
| $M_{\odot}$ | solar mass |
| NS | neutron star |
| EOS | equation of state |

## References

1. Page, D.; Lattimer, J.M.; Prakash, M.; Steiner, A.W. Minimal Cooling of Neutron Stars: A New Paradigm. *Astrophys. J. Suppl. Ser.* **2004**, *155*, 623–650. [CrossRef]
2. Lyne, A.G.; Pritchard, R.S.; Graham-Smith, F.; Camilo, F. Very low braking index for the Vela pulsar. *Nature* **1996**, *381*, 497–498. [CrossRef]
3. Aschenbach, B.; Egger, R.; Trümper, J. Discovery of explosion fragments outside the Vela supernova remnant shock-wave boundary. *Nature* **1995**, *373*, 587–590. [CrossRef]
4. Manchester, R.N.; Hobbs, G.B.; Teoh, A.; Hobbs, M. The Australia Telescope National Facility Pulsar Catalogue. *Astron. J.* **2005**, *129*, 1993–2006. [CrossRef]
5. Dodson, R.; Legge, D.; Reynolds, J.E.; McCulloch, P.M. The Vela Pulsar's Proper Motion and Parallax Derived from VLBI Observations. *Astrophys. J.* **2003**, *596*, 1137–1141. [CrossRef]
6. Pavlov, G.G.; Shibanov, Y.A.; Zavlin, V.E.; Meyer, R.D. Neutron Star Atmospheres. In *NATO Advanced Science Institutes (ASI) Series C*; Alpar, M.A., Kiziloglu, U., van Paradijs, J., Eds.; Springer: Berlin, Germany, 1995; Volume 450, p. 71.
7. Pavlov, G.G.; Zavlin, V.E.; Sanwal, D.; Burwitz, V.; Garmire, G.P. The X-Ray Spectrum of the Vela Pulsar Resolved with the Chandra X-Ray Observatory. *Astrophys. J. Lett.* **2001**, *552*, L129–L133. [CrossRef]
8. Mori, K.; Hailey, C.J.; Paerels, F.; Zane, S. XMM-Newton observations of the Vela pulsar. *Adv. Space Res.* **2004**, *33*, 503–506. [CrossRef]
9. Manzali, A.; De Luca, A.; Caraveo, P.A. Phase-resolved Spectroscopy of the Vela Pulsar with XMM-Newton. *Astrophys. J.* **2007**, *669*, 570–578. [CrossRef]
10. Viganò, D.; Rea, N.; Pons, J.A.; Perna, R.; Aguilera, D.N.; Miralles, J.A. Unifying the observational diversity of isolated neutron stars via magneto-thermal evolution models. *Mon. Not. R. Astron. Soc.* **2013**, *434*, 123–141. [CrossRef]
11. Potekhin, A.Y.; Pons, J.A.; Page, D. Neutron Stars—Cooling and Transport. *Space Sci. Rev.* **2015**, *191*, 239–291. [CrossRef]
12. Potekhin, A.Y.; Chabrier, G. Magnetic neutron star cooling and microphysics. *Astron. Astrophys.* **2018**, *609*, A74. [CrossRef]
13. Ofengeim, D.D.; Yakovlev, D.G. Analytic description of neutron star cooling. *Mon. Not. R. Astron. Soc.* **2017**, *467*, 3598–3603. [CrossRef]
14. Potekhin, A.Y.; Yakovlev, D.G.; Chabrier, G.; Gnedin, O.Y. Thermal Structure and Cooling of Superfluid Neutron Stars with Accreted Magnetized Envelopes. *Astrophys. J.* **2003**, *594*, 404–418. [CrossRef]
15. Potekhin, A.Y.; Chabrier, G.; Yakovlev, D.G. Internal temperatures and cooling of neutron stars with accreted envelopes. *A&A* **1997**, *323*, 415–428.
16. Beznogov, M.V.; Potekhin, A.Y.; Yakovlev, D.G. Diffusive heat blanketing envelopes of neutron stars. *Mon. Not. R. Astron. Soc.* **2016**, *459*, 1569–1579. [CrossRef]
17. Yakovlev, D.G.; Ho, W.C.G.; Shternin, P.S.; Heinke, C.O.; Potekhin, A.Y. Cooling rates of neutron stars and the young neutron star in the Cassiopeia A supernova remnant. *Mon. Not. R. Astron. Soc.* **2011**, *411*, 1977–1988. [CrossRef]
18. Yakovlev, D.G.; Kaminker, A.D.; Gnedin, O.Y.; Haensel, P. Neutrino emission from neutron stars. *Phys. Rep.* **2001**, *354*, 1–155. [CrossRef]

19. Beznogov, M.V.; Yakovlev, D.G. Statistical theory of thermal evolution of neutron stars. *Mon. Not. R. Astron. Soc.* **2015**, *447*, 1598–1609. [CrossRef]
20. Ofengeim, D.D.; Fortin, M.; Haensel, P.; Yakovlev, D.G.; Zdunik, J.L. Neutrino luminosities and heat capacities of neutron stars in analytic form. *Phys. Rev. D* **2017**, *96*, 043002. [CrossRef]
21. Fruscione, A.; McDowell, J.C.; Allen, G.E.; Brickhouse, N.S.; Burke, D.J.; Davis, J.E.; Durham, N.; Elvis, M.; Galle, E.C.; Harris, D.E.; et al. CIAO: Chandra's data analysis system. In *Society of Photo-Optical Instrumentation Engineers (SPIE) Conference Series*; International Society for Optics and Photonics: Washington, DC, USA, 2006; Volume 6270, p. 62701V.
22. Freeman, P.; Doe, S.; Siemiginowska, A. Sherpa: A mission-independent data analysis application. In *Astronomical Data Analysis, Proceedings of the International Symposium on Optical Science and Technology; San Diego, CA, USA, 2001*; Starck, J.L., Murtagh, F.D., Eds.; SPIE Digital Library: Bellingham, WA, USA, 2001; Volume 4477, pp. 76–87.
23. Ho, W.C.G.; Potekhin, A.Y.; Chabrier, G. Model X-Ray Spectra of Magnetic Neutron Stars with Hydrogen Atmospheres. *Astrophys. J. Suppl. Ser.* **2008**, *178*, 102–109. [CrossRef]
24. Biryukov, A.; Astashenok, A.; Beskin, G. Refinement of the timing-based estimator of pulsar magnetic fields. *Mon. Not. R. Astron. Soc.* **2017**, *466*, 4320–4331. [CrossRef]
25. Fortin, M.; Providência, C.; Raduta, A.R.; Gulminelli, F.; Zdunik, J.L.; Haensel, P.; Bejger, M. Neutron star radii and crusts: Uncertainties and unified equations of state. *Phys. Rev. C* **2016**, *94*, 035804. [CrossRef]
26. Akmal, A.; Pandharipande, V.R.; Ravenhall, D.G. Equation of state of nucleon matter and neutron star structure. *Phys. Rev. C* **1998**, *58*, 1804–1828. [CrossRef]
27. Potekhin, A.Y.; Fantina, A.F.; Chamel, N.; Pearson, J.M.; Goriely, S. Analytical representations of unified equations of state for neutron-star matter. *Astron. Astrophys.* **2013**, *560*, A48. [CrossRef]
28. Douchin, F.; Haensel, P. A unified equation of state of dense matter and neutron star structure. *Astron. Astrophys.* **2001**, *380*, 151–167. [CrossRef]
29. Page, D.; Applegate, J.H. The cooling of neutron stars by the direct URCA process. *Astrophys. J.* **1992**, *394*, L17–L20. [CrossRef]
30. Gusakov, M.E.; Kaminker, A.D.; Yakovlev, D.G.; Gnedin, O.Y. The cooling of Akmal-Pandharipande-Ravenhall neutron star models. *Mon. Not. R. Astron. Soc.* **2005**, *363*, 555–562. [CrossRef]
31. Kaminker, A.D.; Kaurov, A.A.; Potekhin, A.Y.; Yakovlev, D.G. Thermal emission of neutron stars with internal heaters. *Mon. Not. R. Astron. Soc.* **2014**, *442*, 3484–3494. [CrossRef]
32. Potekhin, A.Y. Atmospheres and radiating surfaces of neutron stars. *Physics Uspekhi* **2014**, *57*, 735–770. [CrossRef]
33. Nättilä, J.; Steiner, A.W.; Kajava, J.J.E.; Suleimanov, V.F.; Poutanen, J. Equation of state constraints for the cold dense matter inside neutron stars using the cooling tail method. *Astron. Astrophys.* **2016**, *591*, A25. [CrossRef]
34. Ofengeim, D.D.; Kaminker, A.D.; Klochkov, D.; Suleimanov, V.; Yakovlev, D.G. Analysing neutron star in HESS J1731-347 from thermal emission and cooling theory. *Mon. Not. R. Astron. Soc.* **2015**, *454*, 2668–2676. [CrossRef]
35. Friman, B.L.; Maxwell, O.V. Neutrino emissivities of neutron stars. *Astrophys. J.* **1979**, *232*, 541–557. [CrossRef]
36. Voskresensky, D.N. Neutrino Cooling of Neutron Stars: Medium Effects. In *Physics of Neutron Star Interiors*; Blaschke, D., Glendenning, N.K., Sedrakian, A., Eds.; Lecture Notes in Physics; Springer: Berlin, Germany, 2001; Volume 578, p. 467.
37. Blaschke, D.; Grigorian, H.; Voskresensky, D.N. Cooling of neutron stars. Hadronic model. *Astron. Astrophys.* **2004**, *424*, 979–992. [CrossRef]
38. Suleimanov, V.F.; Klochkov, D.; Poutanen, J.; Werner, K. Probing the possibility of hotspots on the central neutron star in HESS J1731–347. *Astron. Astrophys.* **2017**, *600*, A43. [CrossRef]